PERGAMON

International Journal of Multiphase Flow 27 (2001) 1259–1269

International Journal of Multiphase Flow

www.elsevier.com/locate/ijmulflow

Axial viewing studies of horizontal gas–liquid flows with low liquid loading

S. Badie, C.J. Lawrence, G.F. Hewitt *

Department of Chemical Engineering and Chemical Technology, Imperial College of Science, Technology and Medicine, Prince Consort Road, London SW7 2BY, UK

Received 29 August 2000; received in revised form 20 December 2000

Abstract

An axial viewing system is described which was used to investigate the behaviour of the liquid phase in two-phase gas–liquid flows in a 0.079 m diameter horizontal pipe. The region investigated was that of flows with relatively high gas velocities and low liquid loading. Such flows are typically experienced in gas-condensate lines. Axial images obtained using the new system, show that the bulk of the liquid flows within a layer at the bottom of the pipe; however, at higher gas or liquid velocities, a significant portion is entrained as droplets within the gas core and is seen to deposit around the pipe periphery. A process that appeared to contribute significantly to the entrainment was captured using a high speed video recording system. Waves on the liquid layer were observed to converge and breakup into rapidly moving spray droplets. This process appeared to be random, but more frequent with increase in gas or liquid velocities. Secondary droplet breakup was also observed; large droplets were seen to balloon out and burst. The video evidence obtained using the axial viewing method, clearly identified the process of entrainment and deposition as the dominant contributor to the liquid phase transfer to the upper part of the pipe wall.

Keywords: Low liquid loading; Axial images; Entrained droplets; Two-phase flow

1. Introduction

Multiphase flow in pipelines is frequently experienced in the petroleum, chemical and nuclear industries. In the work presented here, particular attention is paid to two-phase gas–liquid flows with low liquid loading, addressing the phenomena experienced in gas-condensate lines. Condensation of the heavier fractions, resulting from reduction in pressure and temperature along the line, leads to the formation of a small quantity of liquid. At high gas flowrates, the liquid flows

* Corresponding author.

0301-9322/01/$ - see front matter
PII: S0301-9322(01)00002-7

partly as a layer on the pipe wall and partly as drops entrained in the gas phase. A number of mechanisms have been proposed for the distribution of the liquid phase but none of them have been supported conclusively. The axial viewing technique was selected as a tool to elucidate the complex nature of these flows. In this technique, the flow is viewed along the axis of the pipe. This technique has been previously applied to both vertical and horizontal multiphase flow systems (Arnold and Hewitt, 1967; Hewitt and Roberts, 1969; Fisher and Yu, 1975; Suzuki and Ueda, 1977; Whalley et al., 1977; Fisher et al., 1978; Whalley et al., 1979; Mayinger, 1981; McQuillan et al., 1985; Shibata et al., 1999). Previous researchers found that it was of considerable value to directly observe the flow in this manner. In the present work, the Imperial College WASP high pressure multiphase flow facility (Davies, 1992; Hall, 1992; Manolis, 1995) was used. To apply the axial view method to this facility, a special design of viewing device was required. Section 2 presents a brief review of previous studies using the axial viewing technique. The in-line axial viewing system commissioned on the WASP facility is outlined in Section 3, and images obtained using this technique are presented and discussed in Section 4.

2. Background

The axial viewing technique was first developed at the UK Atomic Energy Research Establishment, Harwell. The first design (Arnold and Hewitt, 1967) was fitted on top of a vertical Perspex tube with an internal diameter of $1\frac{1}{4}$ in. (32 mm). Annular air–water flows were set up by introducing the air at the bottom of the vertical pipe and injecting water around the periphery using a porous wall section. Axial view images of the flow up the pipe were captured using still photography and high speed filming at frame rates of 2000–4000 per second. This device allowed many significant flow features to be observed clearly for the first time including the motion of the disturbance waves, the entrainment of the droplets and the radial component of the motion of the droplets in the gas stream. Still photographs of vertical annular flow captured by the authors clearly identify disturbance waves and entrained liquid behaviour in the gas core. The authors concluded that this technique has great potential in elucidating many of the unknown phenomena in annular two-phase flow.

Hewitt and Roberts (1969) used the same device to investigate the liquid film interface behaviour and the motion of droplets in vertical annular two-phase flow. Using single-shot flash photography they obtained pictures with excellent definition showing clearly the disposition of droplets in the gas core and the variation of film thickness around the circumference of the pipe.

This facility was modified by Whalley et al. (1977) to investigate wave phenomena in annular two-phase flows. The principal changes were an 8° tilt of the camera and a longer illumination length of 100 mm compared to the 6 mm used previously. With these changes, the events near the tube wall were visible for some distance along the tube. Still photographs and high speed cine films (4000 frames per second) were captured showing the continuously varying wave system. Still and high speed cine stereo photography were also used, allowing the motions of the waves and drops to be observed in three-dimension.

Whalley et al. (1979) used a parallel light technique in their photographic studies of two-phase annular flows. A laser optics technique was used to generate a parallel light beam which passed upwards through the test section. The theory behind this technique is that any object in the light

beam will cast a shadow with a size that is unaffected by its position in the beam. Neglecting the wave nature of light, the object would cast a perfectly sharp shadow if the light beam were truly parallel. Extensive work was carried out to follow the motion of individual droplets and to estimate the transverse droplet velocities. Most of the drops were found to move in a straight line after breaking off from the film. For the cases studied, it was estimated that the maximum transverse velocities of the drops were of the order of 1 m s^{-1}. The velocity measurements were based on the displacement of drops between successive frames of cine film. A review of the optical methods developed at Harwell, including the various axial view systems, was given by Hewitt and Whalley (1980).

Fisher and Yu (1975) used the axial viewing technique to obtain detailed descriptions of flow patterns in horizontal flows. Based on the original idea reported by Hewitt and Roberts (1969), the axial viewing system was fitted onto a 50 mm internal diameter experimental facility to investigate horizontal air–water flows. Continuing this work, Fisher et al. (1978) developed a new axial viewer for a 32 mm internal diameter facility for use with Freon-12 at pressures up to 40 bar. The main use of the axial viewers in both studies was to observe and then describe two-phase flow patterns. In the latter study, the axial viewer was used in conjunction with film thickness and voidage probes to determine the boundaries between different flow patterns.

In an investigation of flooding phenomena in vertical counter-current two-phase flows, Suzuki and Ueda (1977) used the axial viewing technique to observe the state of the wavy liquid surface and the process of flooding. Axial viewing photographs were obtained by installing a high speed camera at the *bottom* of a 28.8 mm internal diameter vertical tube. Small amplitude ripples that were observed at zero gas velocity were seen to grow larger with increases in the gas flowrate. At a certain wave height, the large waves began to extend in the circumferential direction and partially broke up. Sample photographs illustrate the formation of these waves followed by the breakup of a portion of the wave into liquid droplets.

More recently, Shibata et al. (1999) employed axial viewing methods to study the generation and behaviour of entrained droplets. A high speed video camera was simply placed above a vertical test section, 100 mm in diameter, to record images of counter-current flows for an air–water system. Interesting images were obtained, showing the generation of droplets from the film layer and the secondary breakup of large drops in the gas core region.

3. WASP in-line axial viewing system

After carefully studying the past designs of axial viewers, it was decided to base the current design on the axial viewing system used by Fisher and Yu (1975) for air–water tests. However, the original design was complex to machine and not very flexible should there be any need to make alterations. A number of alternative designs were proposed and evaluated before deciding upon the simplest design, shown in Fig. 1.

The flow was viewed at the illuminated plane from the position of the 'eye' shown in the diagram. Downstream of the illuminated plane, the flow from the 3 in. (77.92 mm) nominal bore WASP test section is horizontally divided into two 3 in. tubes to provide space for the viewing and purge systems. The viewing tube was inserted at the junction, with purge air blowing against the direction of the main flow to keep this tube clear of liquid. The camera system was designed to focus on the illuminated plane which was 1.2 m upstream of the bifurcation as illustrated in Fig. 1.

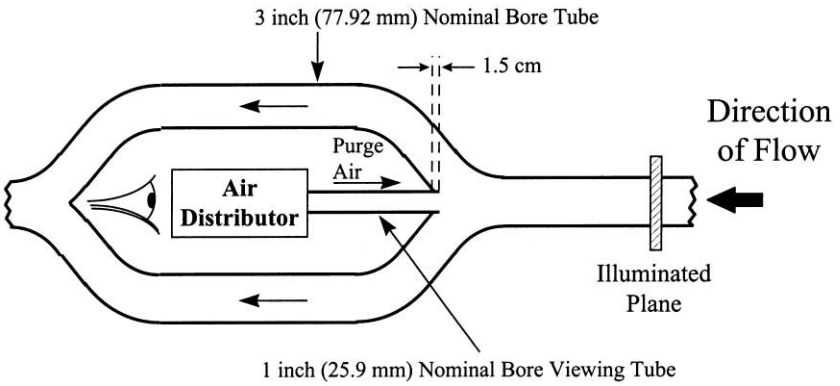

Fig. 1. The basic design of the in-line axial viewing system.

The main body of the viewer was created by welding together a number of 3 in. (77.92 mm) nominal bore stainless steel sections. Eight 45° long-radius elbows, four short straight pipe sections and two longer straight sections were used in this construction.

The 1 in. (25.4 mm) viewing tube was welded to the main section so that it protruded about 1.5 cm into the section as shown in Fig. 1. The small protrusion provides a platform so that any liquid on the upper wall of the main section can drain around the viewing tube, rather than into it. A flange was welded onto the other end of the viewing tube so that the air distributor could be connected.

The main design constraint was to keep entrained liquid drops from reaching the viewing window inside the air distributor. This was addressed by choosing appropriate values for the purge velocity and the length of the viewing tube. The equation used by Fisher et al. (1978) to model the motion of liquid droplets was used to calculate stopping distances for drops travelling against the purge flow. A separate air supply line was constructed, taking a portion of the air supplied to the WASP facility and feeding this to the air distributor via a flexible hose (see Fig. 3). Within the distributor, air first flows back towards the viewing window and then turns into the viewing tube flowing against the direction of the main flow as shown in Fig. 2.

A Kodak EktaPro HG Imager – Model 2000 high speed digital camera was used with a Tarcus TV Zoom Lens 1:2/[11.5–90] to capture images at framing rates of up to 2000 per second. The camera was attached at a right angle to the main section using a frame that allows for adjustment in height and horizontal position. A surface-reflecting mirror was fitted behind the viewing window at the back of the air distributor to reflect the image through 90° towards the camera.

3.1. Operation of the axial viewing system

The WASP experimental facility is shown schematically in Fig. 3. The rig consists of a 37 m long, 78 mm internal diameter tubular stainless steel test section that can be used in the horizontal or slightly inclined (+2° to −2°) orientations. The liquid phases used were Shell Tellus 22 oil (density: 865 kg m^{-3}, viscosity: 40 mPas, surface tension: 32 mN m^{-1} at 23.5°C) and water (density: 1000 kg m^{-3}, viscosity: 1 mPas, surface tension: 37 mN m^{-1} at 23.5°C). The required

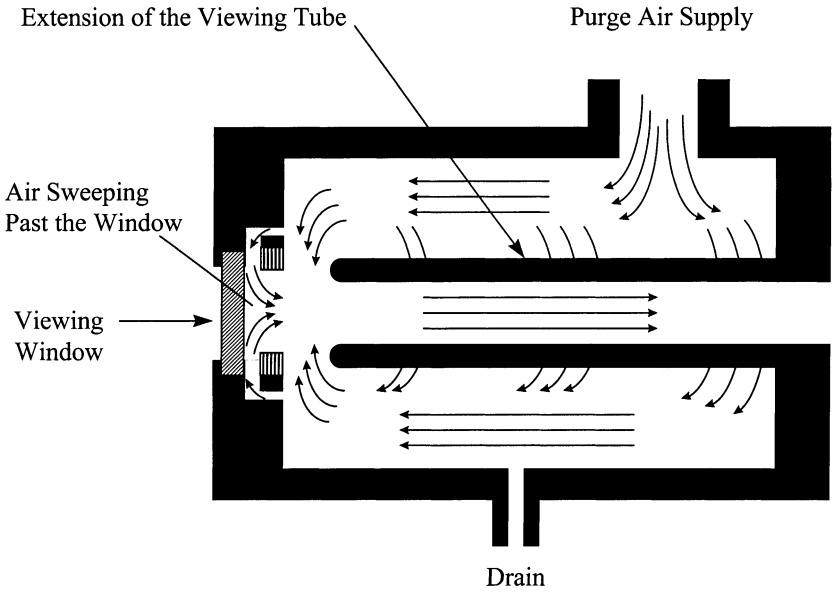

Fig. 2. Side view of the air distributor.

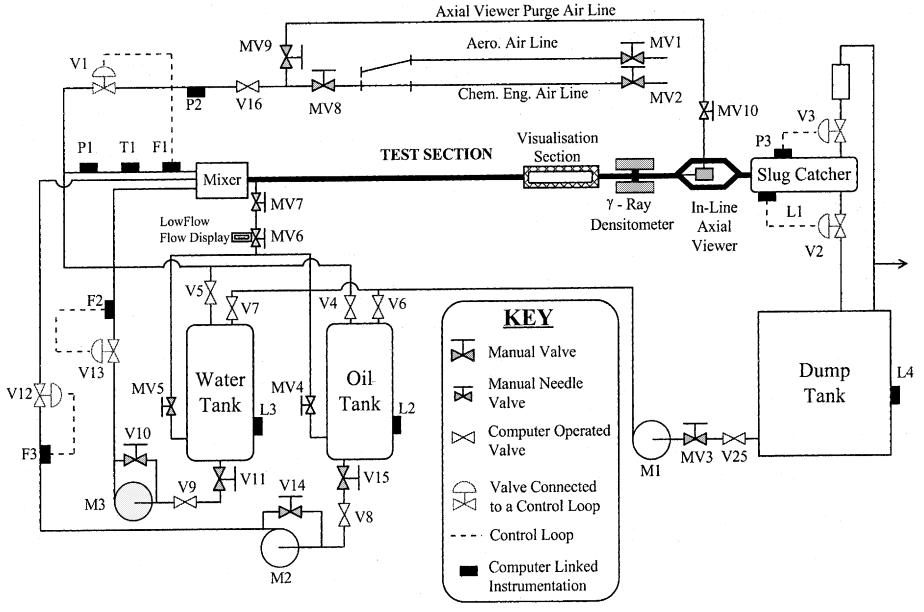

Fig. 3. Schematic diagram of the WASP facility.

liquid phase was fed to the testline from respective 5000 l storage tanks. The air supply was obtained from the adjacent Aeronautics Department's 65 m^3 high pressure tanks supplying air at 30 bar(g).

The WASP facility was operated in the 'blowdown' mode in which high pressure air from the supply tanks flows through the test section and is released to atmosphere. The slug catcher acts as a primary separator of the gas and the liquid phases; the air is discharged through a silencer while the liquid phases are returned to the dump tank where (in the case where two liquid phases are employed) they are separated under the action of gravity before being returned to their respective feed tanks. In the present experiments, only one liquid phase (oil or water) was used.

The present tests were performed with the test section horizontal and with atmospheric pressure at the exit. The air superficial velocity ranged from 15 to 25 m s^{-1}, with the liquid superficial velocity from 0.005 to 0.04 m s^{-1}. For a complete description of the experiments see Badie (2000).

The axial viewing system was installed at the end of the test section just before the outlet gas–liquid separator (slug catcher), as illustrated in Fig. 3. The axial viewing section replaces a straight pipe section of the same length. On the upstream side, a rotating flange was used to connect the section to a section containing a traversing gamma densitometer, upstream of which was an existing visualisation section (see Fig. 3). This visualisation section consisted of a 1 m long, 140 mm outer diameter 78 mm internal diameter polycarbonate tube mounted in a specially constructed stainless steel guard/mounting section with cut-outs to allow viewing and illumination of the transparent polycarbonate section (see Davies, 1992 for details).

The test section was set up so that the visualisation section was about 1.5 m upstream of the viewing window allowing the illumination to take place at any point in the 1 m polycarbonate visualisation section. This offered flexibility in terms of the position and length of the illuminated section. However, the metal guard around the section caused some difficulty in providing a uniform ring of light, because the large slits on either side of the guard are of different size, allowing different amounts of light through the visualisation section. Nevertheless, the flexibility offered by illuminating through the existing visualisation section outweighed the small non-uniformity in the illumination of the pipe. Two 500 W halogen lamps were used to provide the required illumination.

The normal operating procedure of the WASP facility was adjusted to meet the requirements of the axial viewing system. The main addition to the normal operating procedure was that the purge air was introduced prior to any operation involving liquids. This was to ensure that the air distribution section (see Fig. 2) and particularly the viewing window are kept totally dry. The purge air flow was also continued for some time after the completion of the experiments.

Once the required conditions had been set and steady state reached, the high speed digital camera was used to record the flow at a pre-set frame rate. When the recording was complete, the data stored on-board the camera were downloaded onto the image acquisition computer (Viglen Genie 2 Plus Pentium II). The recorded images could then be played back at various frame rates and were recorded onto video tape.

4. Results and discussion

Several representative images obtained using the high speed camera system are presented here. These were selected from a data set of over 32,000 digital images. The effects of the superficial gas and liquid velocities and of the liquid phase used are captured in Figs. 4–11.

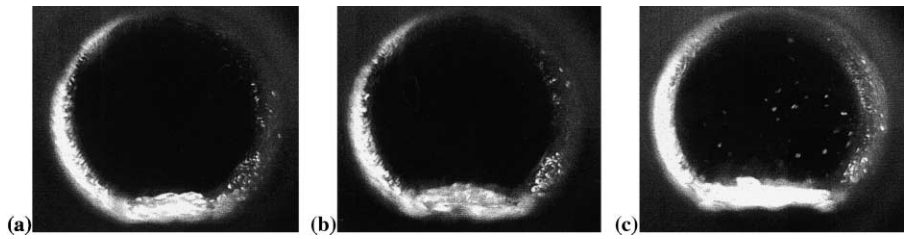

Fig. 4. Images of air–water flow at constant superficial gas velocity of 15 m s^{-1}, showing the effect of superficial liquid velocity: (a) $u_{L,S} = 0.01$ m s^{-1}; (b) $u_{L,S} = 0.02$ m s^{-1}; (c) $u_{L,S} = 0.036$ m s^{-1}.

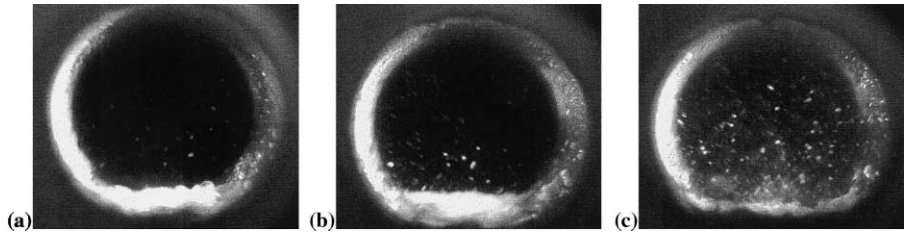

Fig. 5. Images of air–water flow at constant superficial gas velocity of 20 m s^{-1}, showing the effect of superficial liquid velocity: (a) $u_{L,S} = 0.01$ m s^{-1}; (b) $u_{L,S} = 0.02$ m s^{-1}; (c) $u_{L,S} = 0.03$ m s^{-1}.

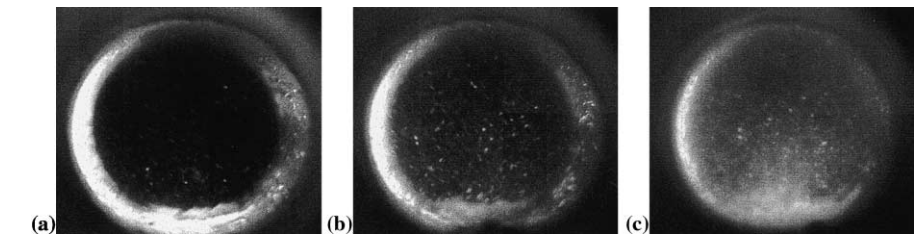

Fig. 6. Images of air–water flow at constant superficial gas velocity of 25 ms^{-1}, showing the effect of superficial liquid velocity: (a) $u_{L,S} = 0.005$ m s^{-1}; (b) $u_{L,S} = 0.01$ m s^{-1}; (c) $u_{L,S} = 0.02$ m s^{-1}.

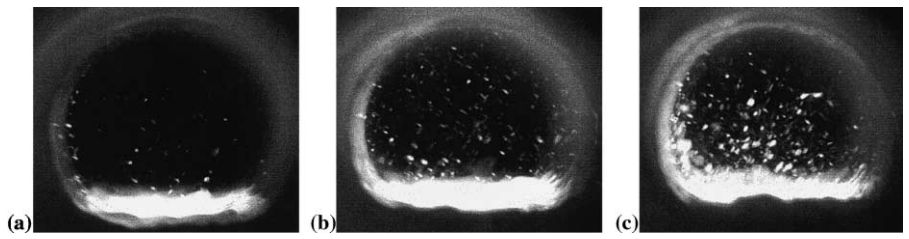

Fig. 7. Images of air–oil flow at constant superficial gas velocity of 15 m s^{-1}, showing the effect of superficial liquid velocity: (a) $u_{L,S} = 0.005$ m s^{-1}; (b) $u_{L,S} = 0.02$ m s^{-1}; (c) $u_{L,S} = 0.03$ m s^{-1}.

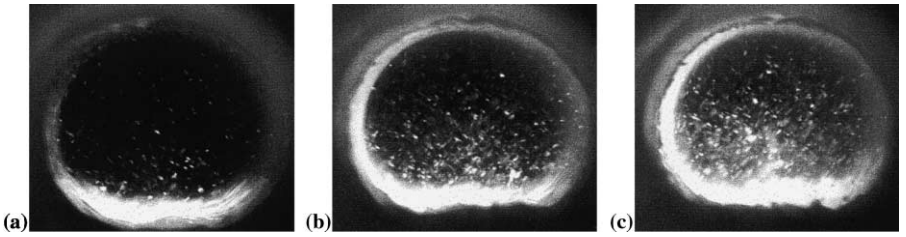

Fig. 8. Images of air–oil flow at constant superficial gas velocity of 20 m s^{-1}, showing the effect of superficial liquid velocity: (a) $u_{L,S} = 0.005$ m s^{-1}; (b) $u_{L,S} = 0.02$ m s^{-1}; (c) $u_{L,S} = 0.03$ m s^{-1}.

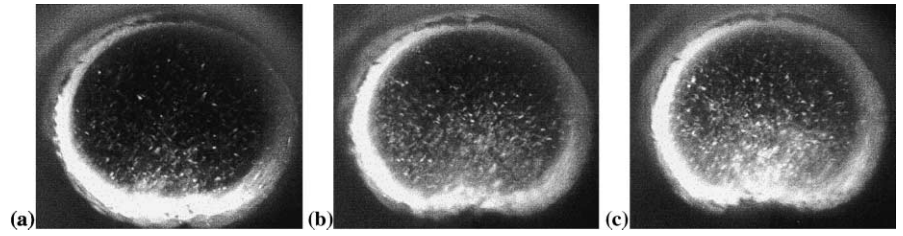

Fig. 9. Images of air–oil flow at constant superifical gas velocity of 25 m s^{-1}, showing the effect of superficial liquid velocity: (a) $u_{L,S} = 0.005$ m s^{-1}; (b) $u_{L,S} = 0.01$ m s^{-1}; (c) $u_{L,S} = 0.02$ m s^{-1}.

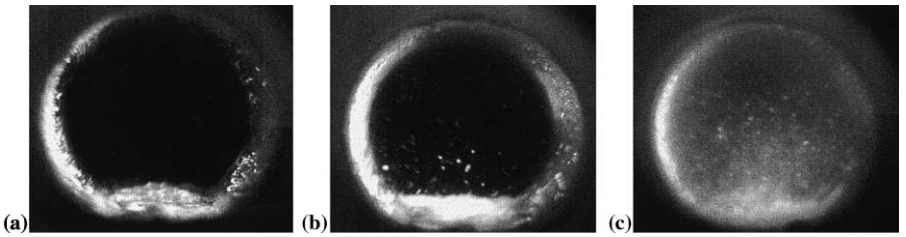

Fig. 10. Images of air–water flow at constant superficial liquid velocity of 0.02 m s^{-1}, showing the effect of superficial gas velocity: (a) $u_{G,S} = 15$ m s^{-1}; (b) $u_{G,S} = 20$ m s^{-1}; (c) $u_{G,S} = 25$ m s^{-1}.

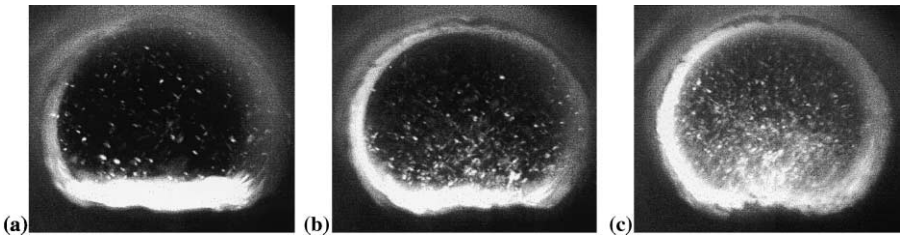

Fig. 11. Images of air–oil flow at constant superficial liquid velocity of 0.02 m s^{-1}, showing the effect of superficial gas velocity: (a) $u_{G,S} = 15$ m s^{-1}; (b) $u_{G,S} = 20$ m s^{-1}; (c) $u_{G,S} = 25$ m s^{-1}.

Figs. 4–9 illustrate the effect of the superficial liquid velocity. Each figure shows three images for the same superficial gas velocity, but increasing superficial liquid velocity. Figs. 4–6 show air–water flows and Figs. 7–9 show air–oil flows. An increase in the liquid velocity at a set gas velocity increases the number of entrained droplets within the gas core. There is also a visible increase in the holdup of the liquid region at the bottom of the pipe with liquid flowrate.

More dramatic changes are observed when the gas velocity is increased at a fixed liquid velocity as shown in Figs. 10 and 11. The liquid holdup decreases markedly and the interface is seen to exhibit greater roughness as the gas velocity is increased. The entrained droplet size decreases with superficial gas velocity, as can be seen in Fig. 11, or by comparing Figs. 4–9. At identical gas and liquid velocities, a much greater number of entrained droplets were seen in the air–oil case compared with the air–water experiments. This can be seen by comparing Figs. 10(b) and 11(b).

The droplet entrainment was observed to derive from waves on the surface of the liquid layer that converge forming a splash that breaks up into rapidly moving spray droplets. Many of these droplets move rapidly across the pipe and deposit around the pipe wall; they are the main contributors to the liquid film on the upper surface of the pipe. A sequence of three frames capturing an explosive discharge of drops is shown in Fig. 12.

The enhancement of entrainment at high gas velocities is probably due to the high interfacial shear stress. The effect of an increase of liquid velocity is to increase the depth and the width of the liquid layer and the propensity for large amplitude waves to form which lead to entrainment. The drop size is a result of the competing influences of surface tension and turbulent stresses in the gas. These stresses tend to disrupt the drops which are therefore smaller at higher gas velocities. The drop size is quite insensitive to the liquid superficial velocity.

Fig. 13 shows separate events that clearly illustrate the ballooning of waves on the liquid to produce a liquid filament before rupturing. Whalley et al. (1979) and more recently Shibata et al.

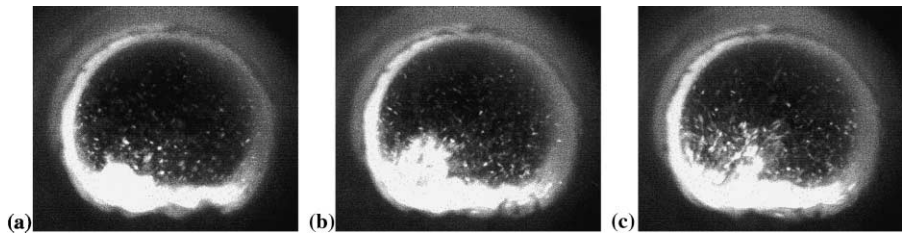

Fig. 12. Successive frames for air–oil flow showing droplet entrainment (superficial gas velocity = 20 m s^{-1}, superficial liquid velocity = 0.02 m s^{-1}): (a) $t = 0$ s; (b) $t = 0.005$ s; (c) $t = 0.010$ s.

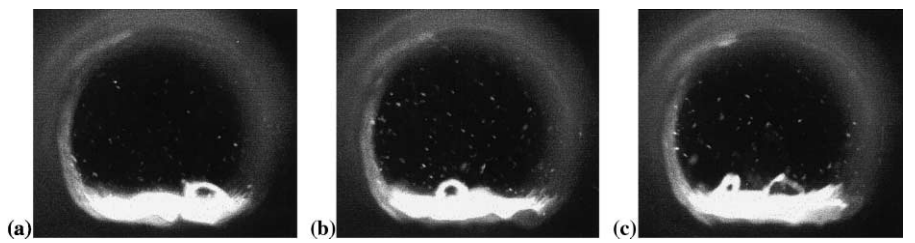

Fig. 13. Images for air–oil flow showing ballooning events in the liquid layer (superficial gas velocity = 15 m s^{-1}, superficial liquid velocity = 0.01 m s^{-1}): (a) $t = 0.186$ s; (b) $t = 0.436$ s; (c) $t = 0.629$ s.

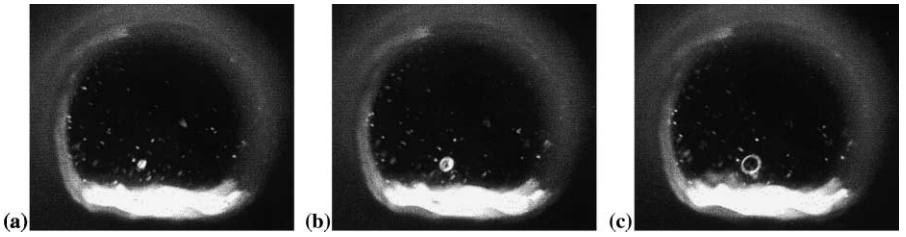

Fig. 14. Successive frames for an air–oil flow showing ballooning of a large drop (superficial gas = 15 m s^{-1}, superficial liquid velocity = 0.01 m s^{-1}): (a) $t = 0$ s; (b) $t = 0.002$ s; (c) $t = 0.006$ s.

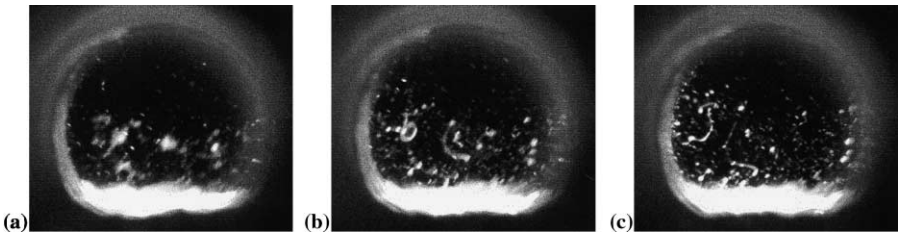

Fig. 15. Successive frames for an air–oil flow showing secondary drop breakup (superficial gas velocity = 15 m s^{-1}, superficial liquid velocity = 0.01 m s^{-1}): (a) $t = 0$ s; (b) $t = 0.008$ s; (c) $t = 0.016$ s.

(1999) included similar images of this phenomenon in their respective publications. The droplets that are produced when the filament ruptures, disperse into the gas core. However these droplets do not exhibit high transverse velocity. Similarly, Fig. 14 shows the ballooning of a large drop to form a ring filament. In the fast moving gas stream, this filament ruptures to produce smaller droplets.

Fig. 15 shows the secondary breakup of large drops in the high speed gas core region. Large drops are thrown into the gas core by the action of the waves in the liquid layer as illustrated in Fig. 12. These drops are unstable and stretch into filaments that breakup into smaller droplets.

5. Conclusions

The interactions between the gas and liquid phases in horizontal stratifying/annular flow are highly complex and not fully understood. However, the axial view studies carried out using the in-line axial viewing system developed in the present work and commissioned on the Imperial College WASP facility, highlighted the important role that the entrained liquid plays in flows with high gas velocities. Spectacular images were obtained, capturing the liquid distribution mechanisms at work in low liquid content, two-phase gas–liquid flows in horizontal pipes. For the relatively large diameter pipe used in the present experiment, the main mechanism responsible for transport of liquid to the top of the pipe is, clearly, the deposition of the entrained droplets. The entrainment process was captured using high speed photography in the axial viewing experiments. Intermittent bursting of waves at the bottom of the pipe is the main contributor to the entrained

liquid phase in the gas core. Once entrained, many of the liquid drops have a significant transverse velocity component that allows them to reach the upper region of the pipe before depositing. It was clear in the video footage that the liquid in the film was draining down the pipe wall and originated solely from droplet deposition. This mechanism has been incorporated in a simple analysis (Badie, 2000) that explains the very large pressure gradients measured (Badie, 2000 and Badie et al., 2000) in these flows, particularly for the oil which has higher viscosity.

Acknowledgements

The authors would like to thank the WASP Consortium for the financial support of this work. In addition, gratitude is extended to Mr S. Fisher, Mr R. King and Mr R. Wallington for their help in design and construction of the Axial Viewing System.

References

Arnold, C.R., Hewitt, G.F., 1967. Further developments in the photography of two-phase gas–liquid flow. The J. Photogr. Sci. 15, 97–114.

Badie, S., 2000. Horizontal stratifying/annular gas–liquid flow. Ph.D. thesis, University of London.

Badie, S., Hale, C.P., Lawrence, C.J., Hewitt, G.F., 2000. Pressure gradient and holdup in horizontal two-phase gas–liquid flows with low liquid loading. Int. J. Multiphase Flow 26, 1525–1543.

Davies, S.R., 1992. Studies of two phase intermittent flow in pipelines. Ph.D. thesis, University of London.

Fisher, S.A., Yu, S.K.W., 1975. Dryout in serpentine evaporators. Int. J. Multiphase Flow 1, 771–791.

Fisher, S.A., Harrison, G.S., Pearce, D.L., 1978. Instrumentation for localised measurements with fast response in liquid/vapour flows. Symposium on Measurements in Polyphase Flows, ASME Winter Annual Meeting, San Francisco, California, USA.

Hall, A.R.W., 1992. Multiphase flow of oil, water and gas in horizontal pipes. Ph.D. Thesis, University of London.

Hewitt, G.F., Roberts, D.N., 1969. Investigation of interfacial phenomena in annular two-phase flow by means of the axial view technique. UK AEA Report, AERE - R6070.

Hewitt, G.F., Whalley, P.B., 1980. Advanced optical instrumentation methods. Int. J. Multiphase Flow 6, 139–156.

Manolis, I.G., 1995. High pressure gas–liquid slug flow. Ph.D. thesis, University of London.

Mayinger, F., 1981. Advanced optical instrumentation. In: Bergles, A.E., Collier, J.G., Delhaye, J.M., Hewitt, G.F., Mayinger, F. (Eds.), Two-phase Flow and Heat Transfer in the Power and Process Industries. Hemisphere Publishing Corporation, Washington, DC, pp. 489–507.

McQuillan, K.W., Whalley, P.B., Hewitt, G.F., 1985. Flooding in vertical two phase flow. Int. J. Multiphase Flow 11, 741–760.

Shibata, Y., Katuyama, A., Kaminaga, F., 1999. The generation and behaviour of entrained droplets in an annular countercurrent two-phase flow in a vertical tube. Two-Phase Flow Modelling and Experimentation, pp. 873–879.

Suzuki, S., Ueda, T., 1977. Behaviour of liquid films and flooding in counter-current two-phase flow – Part 1. Flow in circular tubes. Int. J. Multiphase Flow 3, 517–532.

Whalley, P.B., Hewitt, G.F., Azzopardi, B.J., Pshyk, L., 1977. Axial view photography of waves in annular two-phase flow. UK AEA Report, AERE-R8787.

Whalley, P.B., Hewitt, G.F., Terry, J.W., 1979. Photographic studies of two-phase flow using a parallel light technique. UK AEA Report, AERE-R9389.